AIAA JOURNAL
Vol. 33, No. 7, July 1995

Dynamics of the Juncture Vortex

M. Javed Khan,* Anwar Ahmed,† and J. Randall Trosper*
Texas A&M University, College Station, Texas 77843

Detailed characteristics of the horseshoe vortex system formed at the juncture of a wing and flat plate have been studied using flow visualization and image analysis techniques. With increasing Reynolds number the flowfield exhibited three distinct modes consisting of 1) steady vortex system, 2) oscillatory vortex motion, and 3) vortex shedding. Vortex splitting and subsequent reconnection phenomena were also observed. Different trends in the variation of characteristic frequency were observed when the flow switched from second mode to the third mode.

Introduction

THE displacement of streamlines due to an obstacle mounted on a flat plate results in secondary flow of the first kind[1] in a nominally two-dimensional flow. Additionally, adverse streamwise pressure gradient imposed by the obstacle results in separation of the boundary layer upstream of the obstacle. This separated stream surface rolls up to form a system of vortices which wrap around the wing and convect downstream forming the familiar horseshoe pattern. As this phenomenon is pressure driven, it is visible for both laminar and turbulent boundary layers. Another type of secondary flow, which is known as secondary flow of second kind,[1] is also present for turbulent boundary layers in corner flows; however, in the case of wing-body juncture flows it has not been observed[2] to play a dominant role.

Because of its complex nature wing-body juncture flow continues to be an area of active research. A number of investigations[2–4] into mean characteristics of the flow have been carried out. However, another important aspect of this flow is the time dependency of coherent structures contained therein. Baker[5] extensively studied the time-dependent nature of the juncture-vortex system of a cylinder-flat plate configuration with cylinder's height/diameter (aspect) ratios of 0.5–2.0. He reported the system to be randomly alternating between a quasisteady mode, a low-frequency oscillatory mode, and a high-frequency oscillatory mode—the third state becoming more common at higher Reynolds numbers. Based on pressure measurements in the plane of symmetry, he also reported that the oscillating vortex system existed above a Reynolds number of 5000 based on diameter of the cylinder. The most complicated system observed by Baker was a six-vortex system which also included a small counter-rotating vortex very close to the leading edge of the cylinder due to flow separation from the face of the cylinder. Baker also referred to Schwind's[6] experiments, who also observed an oscillating system. Tobak and Peake[7] characterized unsteadiness of the phenomenon to be that of a periodic shedding nature with the shed vortex eventually dying due to lack of supply of upstream fluid as it moved toward the obstacle. In a later paper, Baker[8] suggested the presence of only a four-vortex system for a turbulent boundary layer at Reynolds numbers as low as 4000 for aspect ratios of 1.5 and greater. These differences in observations have been attributed by Thomas[9] to the effects of cylinder aspect ratios. He reported a steady vortex system for aspect ratios of 0.5–1.0, whereas the phenomenon reported by Baker[5] and Tobak and Peake[7] was seen by him at higher aspect ratios. Thomas[9] also reported a steady pattern for all aspect ratios below a Reynolds number of 1000. Another phenomenon reported by Thomas was the splitting of the vortex into three parts: forming two legs that convected downstream and reconnected behind the cylinder to form a horseshoe vortex; and the remaining part, which was in the form of a thin loop ahead of the cylinder, appeared to move upstream and be consumed by the arrival of a new vortex. He also reported that approach boundary-layer characteristics did not influence the phenomenon. Both Baker and Thomas have discounted von Karman shedding as a source of excitation for the unsteady behavior. This observation is further supported by the more recent results of Agui and Andreopoulos.[10] Bimodality of velocity histograms in the juncture flow reported by Devenport and Simpson[11] also suggests the presence of an unsteady vortex structure in this region.

Considering the various and at times conflicting observations of juncture flow, an experimental investigation was undertaken to better understand the dynamic characteristics of this phenomenon using a combination of flow visualization and image analyses techniques.

Experimental Setup

All experiments were conducted in the 0.6 × 0.9-m water tunnel of Texas A&M University. This tunnel has a maximum speed of 0.75 m/s with a freestream turbulence of less than 1% at peak velocity. The wing model had an airfoil cross section consisting of a NACA 0020 tail and a 3:2 elliptic nose joined at their maximum thickness location, with a maximum thickness-t_{max} of 50.8 mm and span of 610 mm. The wing was mounted vertically on a horizontal plexi-glass flat plate simulating the body, three chord lengths from the leading edge of the plate. The upper end of the wing remained out of the freesurface to eliminate any end effects, and the effective aspect ratio was 10. The flat plate had a width of 508 mm and a length of 1.5 m and a 1:8 fineness ratio elliptic leading edge and a tapered trailing edge. To avoid the effects of side-wall boundary layers of the water tunnel, the flat plate was supported between two-dimensional inserts made of plexiglass (Fig. 1). Tests were conducted through a Reynolds number (Re) range of 2000–6000 based on maximum thickness of the airfoil. The flow was initially tripped by a 2.0-mm-diam wire installed at the maximum thickness point of the leading edge of the flat plate. However, the range of momentum thickness Reynolds numbers (less than 100) was not adequate for the boundary layer to become fully turbulent and was observed to be transitional at the highest tunnel velocity. Boundary-layer profiles were obtained with the help of Aerometric Inc. fast Fourier transform (FFT) based laser Doppler velocimetry (LDV) system. No discernable differences were found between the profiles measured with and without the trip wire. Therefore, the entire series of tests was repeated without the trip wire, however, the juncture vortex characteristics were observed to be insensitive to the state of the oncoming boundary layer. The displacement thickness varied from 7 to 2.9 mm for the range of Reynolds number tested.

Data Acquisition and Analyses Techniques

Flow visualization techniques were carefully selected to study the juncture vortex[12] and near wall flow. A probe consisting of three 0.127-mm-diam platinum wires strung horizontally and spaced 3 mm apart was used to produce the bubbles. The probe was installed

Received June 14, 1993; presented as Paper 93-3473 at the AIAA 4th Applied Aerodynamics Conference, Monterey, CA, Aug. 9–13, 1993; revision received Aug. 11, 1994; accepted for publication Sept. 16, 1994.

*Graduate Student, Aerospace Engineering Department. Member AIAA.
†Assistant Professor, Aerospace Engineering Department; current address: Aerospace Program, Mechanical Engineering Department, Southern University, Baton Rouge, LA 70813. Member AIAA.

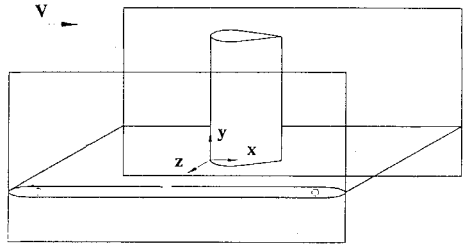

Fig. 1 Schematic of experimental setup.

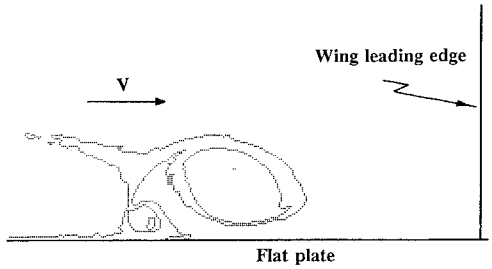

Fig. 2 Example of digitized video image.

on the three-axes traversing system of the tunnel such that the bubble sheets produced by the wires were normal to the oncoming flow and parallel to the flat plate. It was also possible to rotate the probe about the z axis, thus varying the relative distance between the wires. Direct current voltage (up to a maximum of 50 V) could be applied to the wires individually, thereby selectively producing one or more bubble sheets at different heights. Diameter of the bubbles was controlled by varying the applied dc voltage level. A pulsing circuit was also used to produce a pulsed sheet at various frequencies. A 4-W argon-ion laser and a system of beam splitters, mirrors, and cylindrical lenses was used to produce light sheets in the plane of symmetry of the wing, crossflow plane, and horizontal plane. Laser-induced fluorescence was used to capture the surface flow phenomenon. Sodium fluorescein was intermittently injected through a port on the flat plate as a thin sheet which allowed visualization of the near-wall flow very clearly. Flow rate of fluorescein was carefully monitored by a precision metering system. The phenomenon were video taped on a Toshiba SV-F990 video cassette recorder using a set of two NEC TI-23A charge coupled device (CCD) video cameras. Freeze frame/frame advance capabilities of the video cassette recorder were used to study the characteristics in detail.

Trajectory and convective velocity of the vortex system were determined using the Expertvision system from Motion Analysis Inc. The system consisted of Motion Analysis multispeed CCD cameras, 200-Hz video home system (VHS) video recorders, VP320 video processor, Panasonic AG6300 video cassette recorder (VCR), and a Sun SPARCstation work station with Expertvision (EV) and video/analog data collection (VAC) software. The video processor was capable of digitizing video data based on the contrast of the picture. Any point in the picture whose contrast was above a certain threshold was digitized as a 1, or an illuminated pixel. The threshold was adjusted to compensate for varying contrast levels between video passages and, occasionally, between the individual frames of a single passage. Extraneous images were eliminated using the capability of the processor to mask off selected area of the image. Finally, the processor was configured to digitize only the edges of the illuminated areas. These capabilities considerably reduced the computer memory required to store the digitized images.

The VAC program on the SPARCstation was configured to trigger the video processor and digitize an interval of video data varying from a single frame to as many as 10 s at 60 frames/s which was then analyzed by the EV program. Since the objective was to track the movement of the juncture vortex, the wing leading edge, the body surface, and random illuminated particles, hydrogen bubbles were erased creating an edited image of clean data. An example of a digitized image is shown in Fig. 2. The EV software was later used to calculate the centroid of the vortex image for each frame, which was then used to determine the path with reference to a prerecorded video image of a calibrated scale. Streamwise velocity V_x and vertical velocity V_y were obtained by differentiating the path data.

Juncture-Vortex Results and Discussion

For the range of Reynolds number tested, the juncture-vortex system exhibited a very distinct and well-defined Reynolds number dependent behavior. At low Reynolds number the system was observed to be steady. As the Reynolds number was increased the vortex system began to oscillate, and at yet higher Reynolds number vortex shedding was observed. These distinct regimes of behavior, which have been classified as mode I, mode II, and mode III, respectively, are discussed in detail in the following paragraphs.

Starting Flow

As a preliminary step towards understanding the behavior of the juncture-vortex system, its various stages of development were first studied carefully. Figure 3 shows the development of the vortex system as the flow is established in the juncture region. As the purpose of this phase was to qualitatively observe the development of the vortex system, timing information of each frame of the sequence though available has not been included. In these photographs the fluid is marked by hydrogen bubbles from the three platinum wires and streaks of fluorescent dye. As the flow accelerated from rest, the fluid turned down near the wing leading edge toward the flat plate, curled back, and moved upstream (Fig. 3a). This inflow was intercepted by the downstream moving flow resulting in a singular point of boundary-layer separation which gradually strengthened while being pushed farther upstream due to the inflow of outer fluid along the attachment line of the wing. In this process the separated shear layer curled around to form the first of the multiple vortices (Figs. 3a and 3b). As a result of interaction between the upstream moving fluid and the downstream moving fluid layers close to the surface, the system of vortices continued to evolve as the flow accelerated. The flow was observed to have finally settled down into a system of three main vortices (Fig. 3c). The concentration of hydrogen bubbles close to the body surface in Fig. 3c is a counter-rotating flow, hereafter referred to as focus. These foci are an essential part of the evolution of the vortex system. There are two foci associated with this system which are not visible in the Fig. 3c but can be very clearly seen in subsequent figures. The upstream movement of the primary singular point S is evident from Fig. 3. Surface flow visualization with fluorescent dye painted along the attachment line did reveal the presence of a very small corner vortex confirming the observation of Baker.[5]

Although the starting flow passed through phases similar to regimes 1 and 2 described by Schwind,[6] and the two and four vortex systems observed by Baker,[5] these phases could not be seen as a steady phenomena. It should be noted that Baker's four-vortex system essentially consisted of two main vortices with one counter-rotating focus on the flat plate and one very small corner vortex; similarly, his six-vortex system consisted of three main vortices, two counter-rotating foci on the flat plate, and one corner vortex.

Mode I: Steady Mode

Below a Re of 2500 the vortex system remained steady. The three main vortices with two counter-rotating foci were continuously fed by the external flow. Figure 4a shows the plane of symmetry view of this mode, and the plan view is shown in Fig. 4b. The skin friction patterns (and corresponding cartoon) of Fig. 4c very vividly show

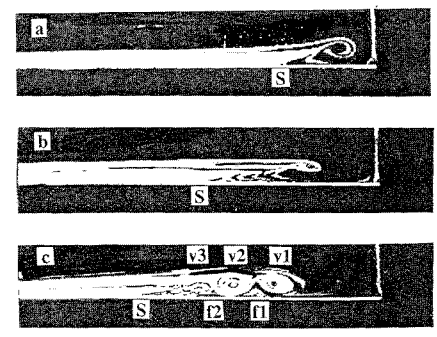

Fig. 3 Sequence of starting flow.

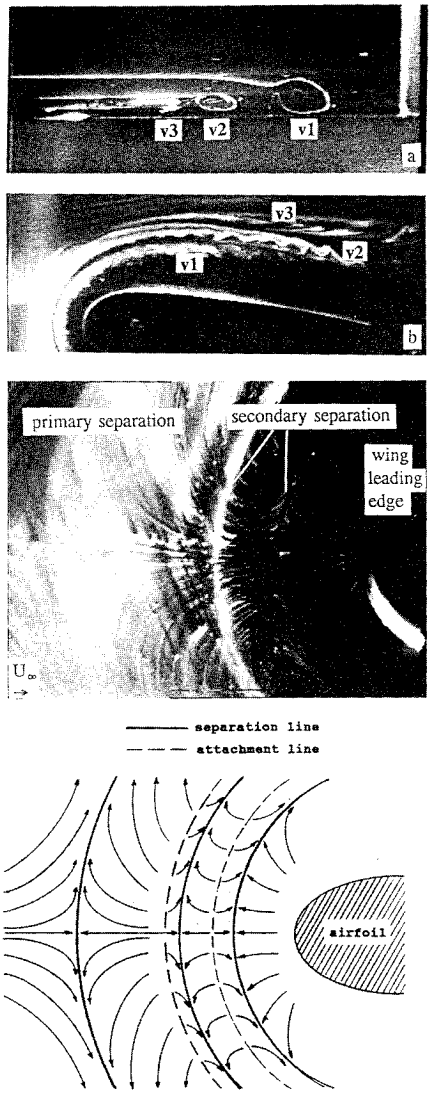

Fig. 4 Mode I: steady vortex system.

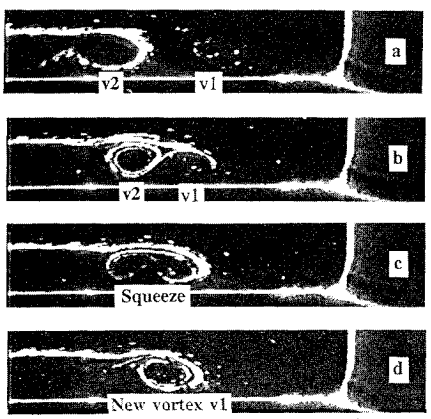

Fig. 5 Mode II: low Reynolds number, engulfment phase.

the primary saddle of separation and the primary and secondary separation lines.

Mode II: Oscillatory Mode

For Re of 2500–3500 the complete vortex system was observed to oscillate back and forth. However, the character of oscillations varied with increasing Reynolds number in this range. The sequence of photographs in Fig. 5 shows that at lower Reynolds numbers, vortex $v1$ after reaching a certain distance downstream started to

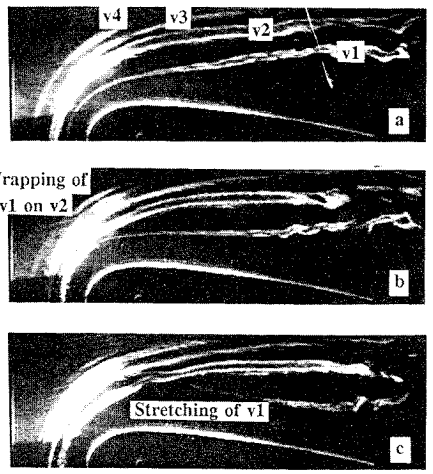

Fig. 6 Mode II: high Reynolds number, wrap-around phase.

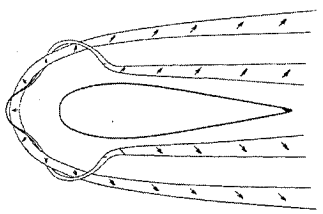

Fig. 7 Sketch of wrap-around phase of mode II.

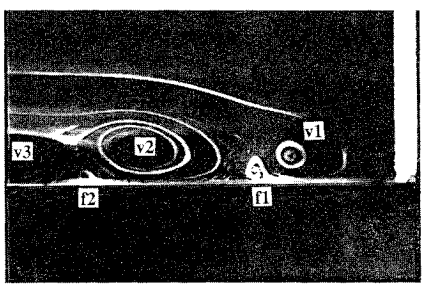

Fig. 8 Mode II: vortices and foci.

travel upstream. After moving upstream vortex $v1$ squeezed vortex $v2$ between itself and vortex $v3$ (not visible in the photograph), while entraining more fluid. Meanwhile, a new vortex ($v4$) was formed farther upstream. The squeezed vortex $v2$ was subsequently engulfed partly by vortex $v1$ and partly by vortex $v3$ to become $v1$-2 and $v2$-3, respectively. After vortex $v1$-2 moved downstream as new vortex $v1$, vortex $v2$-3 became the new vortex $v2$, and vortex $v4$ became vortex $v3$. This cycle then repeated itself.

As the Reynolds number was increased, more and more of vortex $v2$ was observed to merge with vortex $v1$ rather than merging with vortex $v3$. This merged vortex then moved downstream. The maximum downstream convection distance of vortex $v1$ in the plane of symmetry also increased with increasing Reynolds number. This resulted in increased stretching of vortex $v1$. With further increase in Reynolds number, vortex $v1$ wrapped itself around vortex $v2$ (Fig. 6) rather than merging with it. However, as can be seen from Fig. 6 and the sketch of Fig. 7, this wrap around phenomenon was limited to the leading-edge region of the wing. The new vortex $v1$ then moved downstream, thus beginning a new cycle.

The vortex system was, thus, switching between three and four main vortices. The four-vortex phase of the system is visible in Fig. 6.

Observation of the counter-rotating foci $f1$ and $f2$ associated with $v1$ and $v2$ were identified using surface flow visualization and are shown in Fig. 8. These foci clearly showed the oscillatory nature of the vortex system. Figure 9 shows these foci with the hydrogen bubbles turned off to reduce the clutter. As the vortices moved toward each other, focus $f1$ was flattened by vortex $v1$ (Fig. 9c). Just before wrapping of vortex $v1$ around vortex $v2$, focus $f1$, which seemed

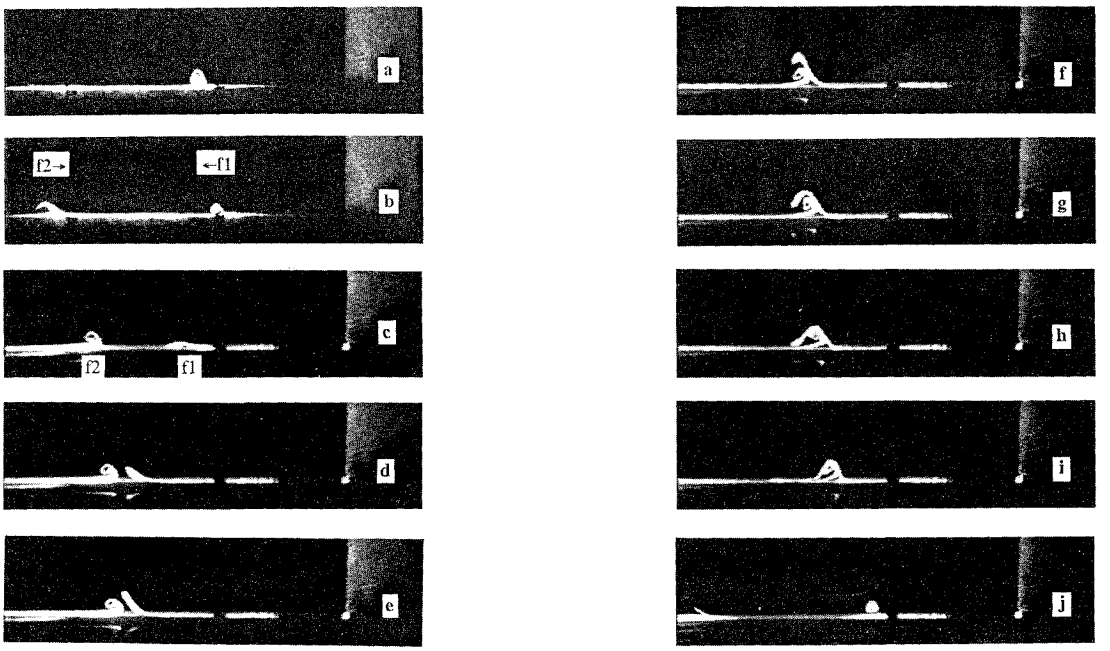

Fig. 9 Oscillation of counter-rotating foci.

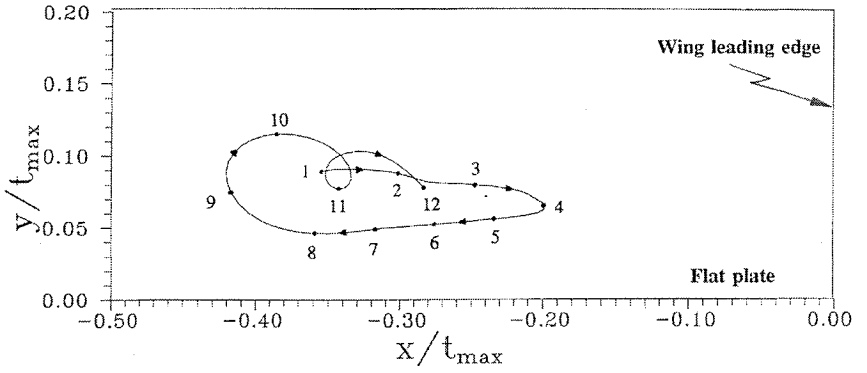

a)

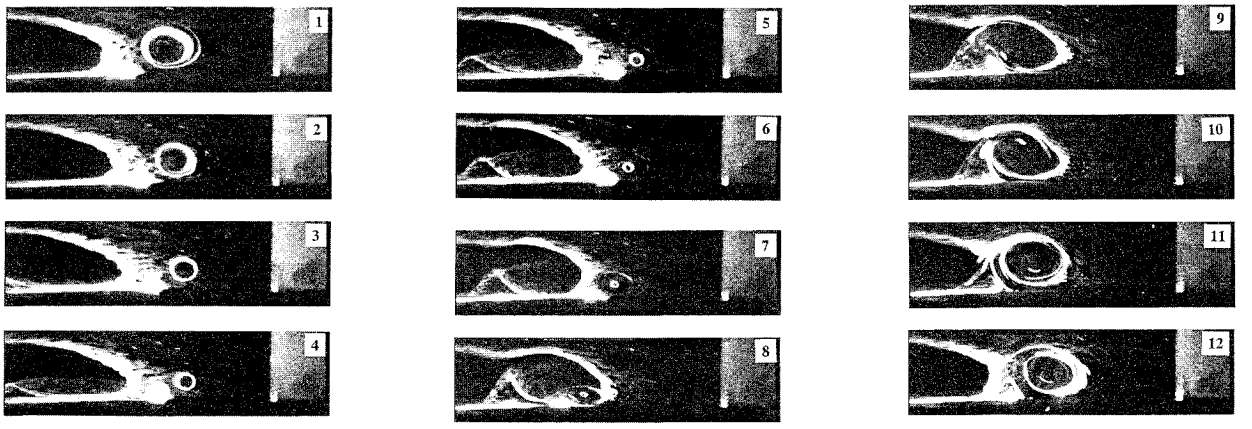

b)

Fig. 10 a) Typical vortex trajectory in mode II, plane of symmetry view, and b) partial video data for vortex trajectory calculations.

like a layer, leap frogged over focus $f2$ (Figs. 9d–9h). During this process the fluid contained in focus $f1$ was distributed between vortex $v2$, focus $f2$, and upstream moving near-wall flow (Fig. 9i), triggering the downstream movement of $v2$ and formation of new $f2$ farther upstream (Fig. 9j). This sequence, without the fluorescent dye, was repeated with the hydrogen bubbles turned on to calculate the juncture-vortex trajectory. A typical trajectory of vortex $v1$ in the plane of symmetry during mode II oscillations is shown in Fig. 10a. The video sequence, which was digitized to produce the trajectory, consisted of 300 frames. This sequence is partially shown in Fig. 10b to identify corresponding positions of the vortex in Fig. 10a. As can now be easily seen, vortex $v1$ steadily moved toward the flat plate as it convected downstream (stations 1–4 labeled on Figs. 10a and 10b). After reaching a maximum streamwise distance of $-0.2t_{max}$, it then convected upstream and wrapped around vortex $v2$ (stations 8–11).

Variations in the convective velocity of the vortex are given in Fig. 11. V_x increased initially to a little over the freestream value and subsequently reduced until the vortex came to a rest at a maximum streamwise location of $-0.2t_{max}$ in the plane of symmetry, though it continued to stretch. The vortex then started to move upstream and accelerated to almost five times the freestream velocity, while moving upstream as it wrapped around $v2$. Changes in V_y were much

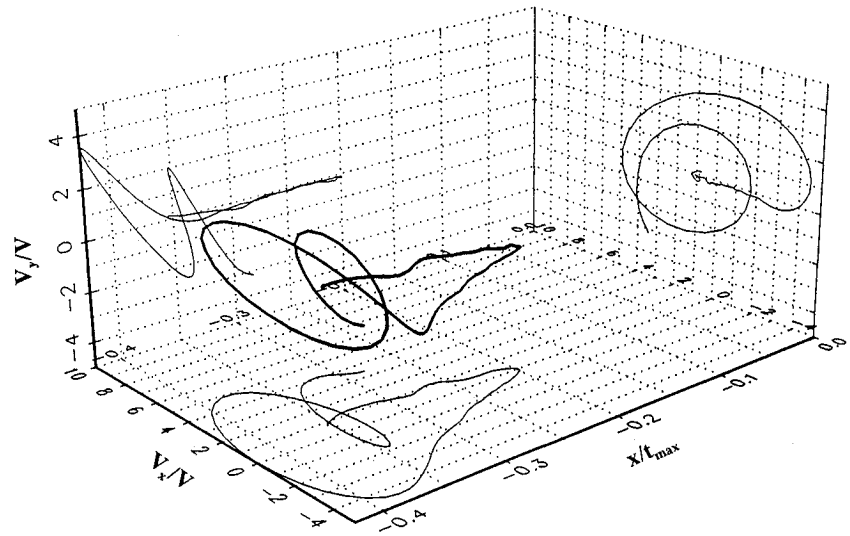

Fig. 11 Variation of vortex velocity in the plane of symmetry.

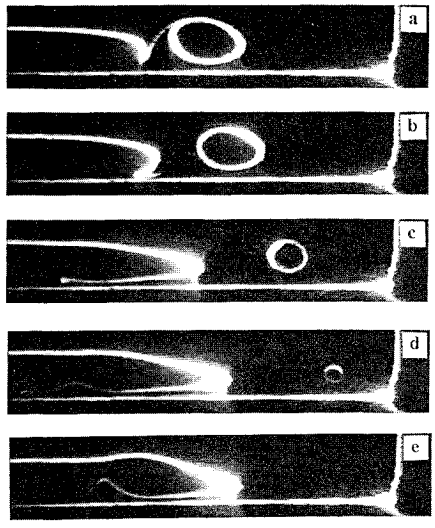

Fig. 12 Mode III: shedding and dissipating phase.

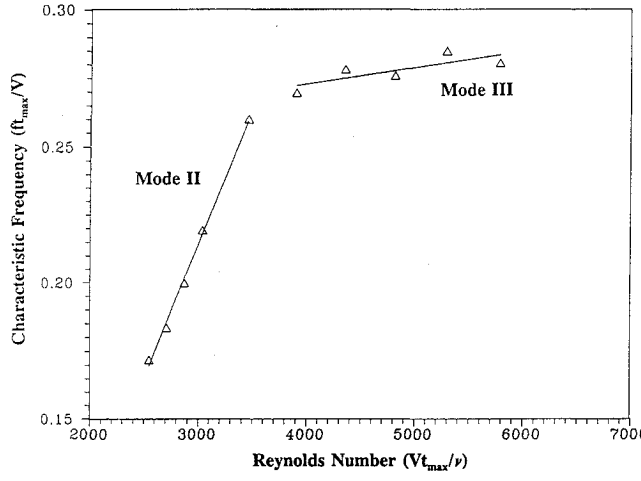

Fig. 13 Variation of characteristic frequency for mode II and mode III.

smaller. The maximum vertical velocity that the vortex achieved during its downstream convection was 16% of the freestream. Further acceleration took place as the vortex changed its direction to move upstream achieving a maximum value of 30% of freestream velocity at the streamwise location of $-0.3t_{max}$, upstream of which it rapidly accelerated as it wrapped around $v2$. Vortex $v1$ was tracked on the periphery of vortex $v2$ and V_y was determined to be almost four times the freestream velocity. The total velocity of vortex $v1$ as well its phase portrait are shown in Fig. 11.

Mode III: Shedding and Splitting Mode

Between *Re* of 3900–6000 (the maximum before the flow became turbulent), vortex $v1$ was observed to shed and stretch while convecting downstream followed by another shed vortex. However, the downstream convection distance of vortex $v1$ had increased to an extent that it became highly stretched in the plane of symmetry and ultimately split due to viscous effects before it could move back upstream to merge with the newly shed vortex (Figs. 12a–12e). Concurrently a new vortex ($v4$) is formed. Thus, the number of vortices in this mode increased to four prior to the splitting of vortex $v1$.

Variation of Characteristic Frequency

Although the characteristic frequency (oscillating/shedding frequency nondimensionalized by freestream velocity and maximum thickness) varied almost linearly with Reynolds number, distinctly different behavior of modes II and III was clearly identifiable (Fig. 13). For mode II, the characteristic frequency varied steeply as compared to its variation in mode III. This behavior provides particularly important insight into the cause of the unsteady nature of the phenomenon and has been attributed by Ahmed and Khan[13] to the leap frogging action of the counter-rotating focus which forces the movement of vortex $v1$. As the whole system convects faster downstream with increasing Reynolds number, the time between the interaction of the foci $f1$ and $f2$ is reduced, thereby increasing the shedding frequency. In mode III as there was no interaction between the foci $f1$ and $f2$, the counter-rotating focus $f2$ had to reach enough strength before it could force vortex $v1$ to shed.

Vortex Splitting and Reconnection

A phenomenon similar to that reported by Thomas[9] for the circular cylinder-flat plate configuration was observed in this investigation also. The photographic sequence of Fig. 14 and sketches of Fig. 15, which are plan views of mode III, shows vortex $v1$ continuing to stretch and eventually splitting near the leading edge under intense axial strain. As the two legs of the vortex convected downstream their split ends moved at a higher velocity than their tail ends and reconnected just past the trailing edge. Observation of this phenomenon clearly showed the process of formation of the so-called fish-tail pattern seen in surface flow visualizations. In the wrap-around phase of mode II reconnection could not be seen due to the limited field of view, however, it is presumed that it takes place farther downstream.

As the reconnected vortex moved downstream, the point of reconnection of the vortex convected at a higher velocity resulting in a rung-like pattern (Figs. 14d and 15d). This pattern seemed to lose

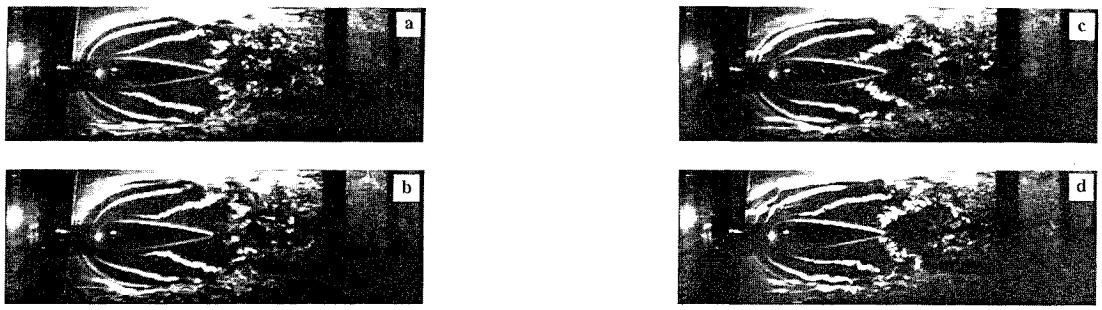

Fig. 14 Vortex splitting and reconnection.

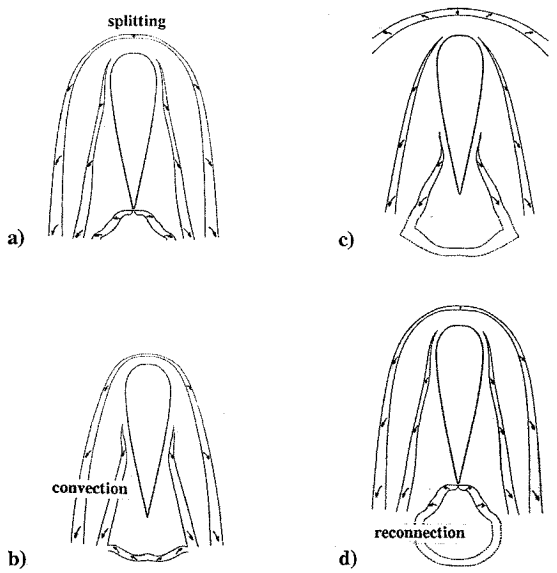

Fig. 15 Sketch of vortex splitting and reconnection phenomenon.

its coherence as it propagated downstream. Although these patterns suggest Crow's instability,[14] details of this phenomenon are being investigated and will be reported in a forthcoming paper.

Conclusions

For the range of Reynolds number tested, the following conclusions are drawn:

1) Wing-body juncture flow consists of three distinct modes, namely, a steady mode, an oscillating mode, and shedding-splitting mode, for the same geometrical configuration.

2) The steady mode consists of three main vortices and two counter-rotating foci associated with them.

3) The oscillating mode consists of three phases, with transition from initial phase in which the second vortex merges with the third vortex as it is squeezed by the upstream moving first vortex, then to merger of the upstream moving vortex and the second vortex, and, finally, to a phase in which the upstream moving vortex wraps around the second vortex. The phenomena of merging/wrapping of the second mode is limited only to the leading-edge region of the wing. In this mode, the system switches between three and four main vortices.

4) Analyses of the vortex trajectory provided detailed information insofar as the motion of the shed vortex in the plane of symmetry is concerned. The vortex moves down toward the flat plate as it convects toward the wing leading edge. The vortex achieves a streamwise velocity of almost two and one-half times the freestream as it moves back upstream just before engulfment, in comparison to its downstream motion which is just a little over the freestream value. The vertical velocity shows a much smaller change as the vortex traces its cyclic path (except when it was engulfed).

5) The shedding-splitting mode consists of a three-/four-vortex system. Prior to the splitting of the shed vortex, a new one is formed, thus increasing the number of vortices to four. In mode III the split vortex reconnects at the trailing edge, forming a rung-like pattern. This is presumably the cause of the fish-tail pattern seen in surface flow visualization studies of juncture flow.

References

[1]Prandtl, L., *Essentials of Fluid Dynamics*, Blackie and Sons, Glasgow, Scotland, UK.

[2]Shabaka, I. M. M. A., and Bradshaw, P., "Turbulence Measurements in an Idealized Wing-Body Junction," *AIAA Journal*, Vol. 10, No. 2, 1981, pp. 131, 132.

[3]Menna, J. D., and Pierce, F. J., "The Mean Flow Structure Around and Within a Turbulent Junction or Horse Shoe Vortex, Part I: The Upstream and Surrounding Three Dimensional Boundary Layer," *Journal of Fluids Engineering*, Vol. 110, Dec. 1988, pp. 406–414.

[4]Abid, R., and Schmitt, R., "Experimental Study of a Turbulent Horse-Shoe Vortex Using Three Component Laser Doppler Velocimeter," AIAA Paper 86-1069, May 1986.

[5]Baker, C. J., "The Laminar Horseshoe Vortex," *Journal of Fluid Mechanics*, Vol. 95, Pt. 2, 1979, pp. 347–367.

[6]Schwind, R., "The Three-Dimensional Layer near a Strut," Gas Turbine Lab. Rept., Massachusetts Inst. of Technology, Boston, 1962.

[7]Tobak, M., and Peake, D. J., "Topology of Two-Dimensional and Three-Dimensional Separated Flows," AIAA Paper 79-1480, July 1979.

[8]Baker, C. J., "The Turbulent Horseshoe Vortex," *Journal of Wind Engineering and Industrial Aerodynamics*, Vol. 6, 1980, pp. 9–23.

[9]Thomas, A. S. W., "The Unsteady Characteristics of Laminar Juncture Flow," *Physics of Fluids*, Vol. 30, Pt. 2, 1987, pp. 283–285.

[10]Agui, J. H., and Andreopoulos, J., "Experimental Investigation of a Three-Dimensional Boundary Layer Flow in the Vicinity of an Upright Wall Mounted Cylinder," *Journal of Fluids Engineering*, Vol. 114, Dec. 1992, pp. 566–576.

[11]Devenport, W. J., and Simpson, R. L., "Time Dependent and Time-Averaged Turbulence Structure near the Nose of a Wing-Body Junction," *Journal of Fluid Mechanics*, Vol. 210, 1990, pp. 23–55.

[12]Delisi, D. P., and Greene, G. C., "Measurement and Implications of Vortex Motions Using Two Flow Visualization Techniques," *Journal of Aircraft*, Vol. 27, No. 11, 1990, pp. 968–971.

[13]Ahmed, A., and Khan, M. J., "On the Role of Counter-Rotating Foci Structures in Wing-Body Juncture Flow," *Bulletin of the American Physical Society*, Vol. 38, No. 10, 1993, p. 2203.

[14]Crow, C. S., "Stability Theory for a Pair of Trailing Vortices," *AIAA Journal*, Vol. 8, No. 12, 1970, pp. 2172–2179.